SANDIA REPORT

Two-Dimensional Green's Function Poisson Solution Appropriate for Cylindrical-Symmetry Simulations

Merle E. Riley

Sandia National Laboratories

SF2900Q(8-81)

DISCLAIMER

Portions of this document may be illegible in electronic image products. Images are produced from the best available original document.

Two-Dimensional Green's Function Poisson Solution
Appropriate for Cylindrical-Symmetry Simulations

Merle E. Riley
Laser, Optics, and Remote Sensing Department
Sandia National Laboratories
P.O. Box 5800
Albuquerque, NM 87185-1423

Abstract

This report describes the numerical procedure used to implement the Green's function method for solving the Poisson equation in two-dimensional (r,z) cylindrical coordinates. The procedure can determine the solution to a problem with any or all of applied voltage boundary conditions, dielectric media, floating (insulated) conducting media, dielectric surface charging, and volumetric space charge. The numerical solution is reasonably fast, and the dimension of the linear problem to be solved is that of the number of elements needed to represent the surfaces, not the whole computational volume. The method of solution is useful in the simulation of plasma particle motion in the vicinity of complex surface structures as found in microelectronics plasma processing applications. This report is a stand-alone supplement to the previous Sandia Technical Report SAND98-0537 presenting the two-dimensional Cartesian Poisson solver.

I. Introduction

The fields about a prescribed distribution of electric charge are solved by superposition once Coulomb's law is introduced. In general though, fields are specified in terms of known voltage boundary conditions, not charge distributions, which requires the solution of partial differential equations or integral equations.[1] Finite difference techniques for solving the Poisson or Laplace equations are standard fare. They require numerical solutions covering the whole computation volume of the problem. An alternative method is to use the Green's function for an unknown source distribution, with sources localized to the surfaces, and to formulate the solution as a Fredholm integral equation of first kind,[2] which becomes a linear algebra problem once discretized. The advantage of the Green's function technique is the smaller dimension of the array of surface unknowns as compared to the number of volume elements filling the whole computation volume. This is illustrated by considering a square of N elements on a side. The Green's function method has 4N unknowns and a 4N by 4N coupling matrix. A finite difference formulation would have N^2 unknowns and a N^2 by N^2 matrix. However the latter matrix is sparse and numerical methods exist to take advantage of the sparseness. Another advantage of the Green's function method is that volume grids are unnecessary in the absence of space charge and that the points of evaluation of the fields within the volume can be arbitrarily positioned.

The Poisson equation (PE) in three dimensions (3D) for the potential field V due to a distribution of charge ρ is

$$\nabla^2 V(\vec{R}) = -\rho(\vec{R})/\varepsilon_o \tag{1}$$

where SI units are used: namely, distance is in m, V is in volts (V), ρ is in C/m^3, and the vacuum permittivity ε_o is in C^2/J m. The PE can be resolved by use of the free-space Green's function:[1,2]

$$G_o(\vec{R}, \vec{R}') = -1/4\pi|\vec{R} - \vec{R}'|,$$
$$\nabla_R^2 G_o(\vec{R}, \vec{R}') = \delta^3(\vec{R} - \vec{R}'), \tag{2}$$

as

2

$$V(\vec{R}) = -\frac{1}{\varepsilon_o} \int d^3 R' \, G_o(\vec{R}, \vec{R}') \rho(\vec{R}')$$

$$= \int d^3 R' \, \rho(\vec{R}') / 4\pi \varepsilon_o |\vec{R} - \vec{R}'| . \tag{3}$$

The form of G_o is chosen to vanish at large distance analogous to the Coulomb field of a charged particle. Homogeneous solutions of the Laplace equation are not superimposed with the PE particular solution, because all fields are due to, or represented as, the superposition of real charges. This carries over to the representation of dielectric media, which are replaced by charged surfaces rather than a space-dependent permittivity, $\varepsilon(\vec{R})$.

A point of importance in the application of the Poisson solver to plasma physics problems is the stiffness that is associated with the light electron mass and relatively high temperature. This is discussed in the Appendix of this report.

II. The Two-Dimensional Poisson Equation in Cylindrical Symmetry

The 2D PE in cylindrical coordinates with imposed rotational symmetry about the z axis may be obtained by introducing a restricted spatial dependence into the PE in Eq.(1) or the Green's function solution as given in Eq.(3). The result is the conversion to 2D coordinates:

$$\rho(\vec{R}) \to \rho(r, z) \equiv \rho(\vec{r}),$$

$$V(\vec{R}) \to V(r, z) \equiv V(\vec{r}). \tag{4}$$

Lower case $\vec{r}$ is used to denote a vector in (r,z) space. The new 2D Green's function is the solution of[2]

$$\left(\frac{\partial^2}{\partial^2 r} + \frac{\partial}{r\,\partial r} + \frac{\partial^2}{\partial^2 z}\right) G(\vec{r},\vec{r}') = \frac{1}{2\pi r}\delta(r-r')\delta(z-z') \equiv \delta^2(\vec{r},\vec{r}'),$$

$$\int d^2 r\; \delta^2(\vec{r},\vec{r}') \equiv 2\pi\int_0^\infty r\,dr \int_{-\infty}^\infty dz\; \delta^2(\vec{r},\vec{r}') = 1,$$

$$G(\vec{r},\vec{r}') \equiv G(r,z;r',z') = \frac{1}{2\pi}\int_0^{2\pi} d\theta\; G_o(\vec{R},\vec{R}'),$$

$$= -\frac{1}{8\pi^2}\int_0^{2\pi} d\theta\Big((z-z')^2 + r^2 + r'^2 - 2rr'\cos(\theta)\Big)^{-1/2}.$$

(5)

Note that the 2D integration and delta function have been defined with the 2π included in the volume element. The last integral in Eq.(5) can be done analytically, resulting in a complete elliptic integral of the first kind.[3] This is only useful because these elliptic integrals have convenient numerical representations as low order polynomial approximations.[3]

The 2D Green's function defined in Eq.(5) may be reduced to

$$G(r,z;r',z') = -\frac{1}{2\pi^2} D_{\max}^{-1} K(m),$$

$$D_{\max}^2 = (z-z')^2 + (r+r')^2 = D_{\min}^2 + 4rr',$$

$$D_{\min}^2 = (z-z')^2 + (r-r')^2,$$

(6)

$$m = 4rr' / D_{\max}^2,$$

$$m_1 = 1 - m = D_{\min}^2 / D_{\max}^2.$$

D_{max} and D_{min} are the maximum and minimum of the separation of the source and observation points as the azimuthal integration angle in Eq.(5) sweeps about the z axis. K is the complete elliptic integral of the first kind, m is the "parameter," and m_1 is the "complementary parameter."[3] The limits of the elliptic integral are known,[3]

$$K(m) \xrightarrow[m \to 0]{} \frac{\pi}{2}\left(1 + \frac{1}{4}m + \frac{9}{64}m^2 + ...\right),$$

$$K(m) \xrightarrow[m \to 1]{} \frac{1}{2}\ln\left(\frac{16}{m_1}\right). \tag{7}$$

These are useful in reconciling the formulae with the Cartesian Green's function and in evaluating the near-field limit. As an example one finds:

$$G(r,z;r',z') \approx \frac{1}{4\pi^2 r}\ln\left(\frac{\sqrt{(z-z')^2 + (r-r')^2}}{8r}\right), \tag{8}$$

$$r \to r', z \to z'.$$

This is similar to the 2D Cartesian Green's function[4], differing only by a factor of $2\pi r$, and with the R_1 constant therein replaced by $8r$ in the present relation. The 2D cylindrical Green's function does not have the same singular properties at both large and small argument as the 2D Cartesian Green's function: at large separation the cylindrical Green's function decays like 1/R just as the Coulomb potential due to a point source.

The potential due to a volume distribution of charge is given by the 2D version of Eq.(3), namely:

$$V(\vec{r}) = -\frac{1}{\varepsilon_o}\int d^2 r'\, G(\vec{r},\vec{r}')\,\rho(\vec{r}'). \tag{9}$$

This distribution and potential are independent of the θ coordinate. In the case that a surface charge is present, say $\sigma(\vec{r})$, in units of C/m^2, the appropriate potential is given by taking a zero-thickness or surface-delta-function limit of a volume charge. Let t be the local coordinate normal to the surface, which is located at t_s, then the substitution of

$$\rho(\vec{r}) = \sigma(\vec{r})\delta(t - t_s) \tag{10}$$

will convert the volume charge integration in Eq.(9) to a surface integration. The solution to the surface-charge problem is given as the 1D integral covering all surfaces:

$$V(\vec{r}) = -\frac{1}{\varepsilon_o} \int ds'\, G(\vec{r},\vec{r}'(s'))\, 2\pi r'(s')\sigma(\vec{r}'(s')), \tag{11}$$

where the 2D vector $\vec{r}' = \vec{r}'(s')$ traces out the surfaces. The path of integration is along the surface, perpendicular to the local surface normal.

It is also necessary to evaluate the electric field produced by all the charges. As the electric field is the negative gradient of the potential, the field can be evaluated from Eqs.(9) and (11). For the volume sources:

$$\vec{E}(\vec{r}) = \frac{1}{\varepsilon_o} \int d^2 r'\, \vec{\nabla}_r G(\vec{r},\vec{r}')\rho(\vec{r}') . \tag{12}$$

Of course the gradient must be evaluated in terms of the elliptic integrals in order to be useful. The general expression for $\vec{\nabla}_r G$ is found to be:

$$\vec{\nabla}_r G(\vec{r},\vec{r}') \equiv \left(\hat{e}_r \frac{\partial}{\partial r} + \hat{e}_z \frac{\partial}{\partial z} \right) G(r,z;r',z')$$

$$= \frac{1}{2\pi^2 D_{max}} \left(\frac{\vec{r} - \vec{r}'}{D_{min}^2} E(m) - \frac{\vec{r}}{2\,r^2}\, (E(m) - K(m)) \right), \tag{13}$$

where the notation is as defined in Eq.(6) except that $E(m)$ is the complete elliptic integral of the second kind.[3] The limiting values of $E(m)$ are known:

$$E(m) \xrightarrow[m \to 0]{} \frac{\pi}{2}\left(1 - \frac{1}{4}m - \frac{3}{64}m^2 + ... \right),$$

$$E(m) \xrightarrow[m \to 1]{} 1 . \tag{14}$$

Eqs.(9) and (11) for the potential, and Eq.(12) for the field together with its analogous surface charge form, constitute all that is needed for the Green's function Poisson

solution. The remaining items to discuss are numerical representations and imposition of boundary conditions.

III. Overall Structure of Solution

The specification of the solution is done by means of voltage boundary conditions on conductors, typically metal surfaces. Metals are at a constant voltage,[1] but with an unknown charge distribution at the surface. These also include highly conductive plasma interfaces. All metals will have an unknown total and surface distribution of charge, except that floating or insulated metal parts will have a fixed total charge and an unknown charge distribution and voltage. Dielectrics will have unknown surface charges to modify the fields inside the media. This takes the form of jump conditions in the normal electric field at the dielectric interface surface. Boundaries that are markers for periodic reflections of the solution will have zero normal field conditions (periodic boundary conditions).

One can see that it is necessary to break all surfaces into finite elements or increments in order to obtain an accurate numerical representation of the quantities that vary along the surfaces. Let all the elements be indexed by j, with the understanding that two materials in contact with a region of their surfaces in common will have just one set of elements in the common region. Each surface element will have a centroid at $\vec{r}_j$, a length ds_j, and a unit normal $\hat{n}_j$. The total area of a surface element is $2\pi r_j\, ds_j$, as the element is swept about the z axis. If there is a volume charge, the volume elements, which are really incremental cross sectional areas that are rotated about the z axis to form a solid ring, will be specified by the centroids $\vec{r}_j$ and the areas dA_j, of incremental volume $2\pi r_j\, dA_j$. No surface or volume element will be allowed to be *centered* on the z axis. It should not be necessary to do so.

Some labels or partitionings will be introduced for the surface elements. Volume elements will be labeled by a "v" in all cases. The surface elements will be labeled with either an "m," denoting a voltage boundary condition as on a metal including floating metals, a "d," denoting a dielectric interface, or an "s" denoting an element in any of the surface partitions. The total number of elements in these partitions is N_v, N_m, N_d, and $N_s = N_m + N_d$.

Consider a system of voltage-specified metal surfaces with a given space charge in the volume. Together Eqs.(9) and (11) relate voltage at the metal surface elements to charges in the volume and on the metal. Without loss of generality, the

integrals can be replaced by numerical quadratures or by sums over finite elements of the surfaces and volume to give the linear algebraic version of the system:

$$V_i^m = \sum_{j \in m} G_{i,j}^{mm} q_j^m + \sum_{j \in v} G_{i,j}^{mv} q_j^v \qquad (15)$$
$$i \in m$$

It is seen that the only unknowns in this linear system of equations are the charges on the metal elements, q_j^m. All the q_j^x are defined as being the total charge (in C) on either a surface or a volume element, which are both 3D figures of revolution obtained by rotation about the z axis of the problem:

$$q_i^s = 2\pi r_i \, ds_i \, \sigma(\vec{r}_i) , \qquad (16)$$
$$q_i^v = 2\pi r_i \, dA_i \, \rho(\vec{r}_i) .$$

It is to be noted that the charges are no longer being represented as charge per length as in the 2D Cartesian method.[4] There are as many unknowns, N_m, as equations in this system described by Eq.(15). The exact procedure of discretizing Eqs.(9), (11), and (12) will be discussed in the next sections. Eq.(15) constitutes a complete definition of the problem as formulated with potential boundary conditions and space charge. The solution of the linear system of equations for the unknown charges on each of the metal elements determines the fields everywhere in space. Note that the number of points involved in evaluating the space charge is not involved in inverting the coefficient matrix in Eq.(15). The accuracy of the solution will be determined by the number and density of elements chosen on the surfaces and volume. The numerical solutions should converge to the exact solution as the density and number of elements increase everywhere.

In contrast to the 2D Cartesian situation, there are no provisions made for periodic boundary condition to be applied in the 2D cylindrically symmetric case. Thus there is no "r" or reflective subset of the boundary finite elements.

The remaining illustration is the dielectric match condition. This takes the form of an inhomogeneous condition on the normal field at each element on a dielectric interface:

$$V_i^d = \sum_{j \in m} {}^n G_{i,j}^{dm} \, q_j^m + \sum_{j \in d} {}^n G_{i,j}^{dd} \, q_j^d + \sum_{j \in v} {}^n G_{i,j}^{dv} \, q_j^v$$

$$= \sum_{j \in s} {}^n G_{i,j}^{ds} \, q_j^s + \sum_{j \in v} {}^n G_{i,j}^{dv} \, q_j^v \quad . \tag{17}$$

$$i \in d$$

The quantity V_i^d is of physical dimension V/m, the same as the electric field. Note that the matrix $G_{i,j}$ is not the same physical dimension as the Green's function G in Eq.(6), as the $-1/\varepsilon_o$ constant in the PE is now included. $G_{i,j}$ is dimension of V/C and G is 1/m. Also ${}^n G_{i,j}^{sx}$ is dimension V/mC. In addition to describing the dielectric match, the d partition also contains the effects of known added amounts of charge to the faces of dielectrics. This details of this will be given later. At the moment, the purpose is to illustrate the form of the total system of equations determining the solution.

Write Eqs.(15) and (17) in vector matrix notation, suppressing the indices:

$$\begin{pmatrix} \mathbf{V}^m \\ \mathbf{V}^d \end{pmatrix} = \begin{pmatrix} \mathbf{G}^{ms} & \mathbf{G}^{mv} \\ {}^n \mathbf{G}^{ds} & {}^n \mathbf{G}^{dv} \end{pmatrix} \begin{pmatrix} \mathbf{q}^s \\ \mathbf{q}^v \end{pmatrix}. \tag{18}$$

This can immediately be rearranged to solve for the unknown charges, $\mathbf{q}^s$:

$$\begin{pmatrix} \mathbf{G}^{ms} \\ {}^n \mathbf{G}^{ds} \end{pmatrix} \left(\mathbf{q}^s \right) = \begin{pmatrix} \mathbf{V}^m \\ \mathbf{V}^d \end{pmatrix} - \begin{pmatrix} \mathbf{G}^{mv} \\ {}^n \mathbf{G}^{dv} \end{pmatrix} \left(\mathbf{q}^v \right). \tag{19}$$

It is to be noted that the partition s contains the partitions m and d, all of which are surface elements with unknown charges. Only the partition m contains known voltages. The volume charges are known, as are added dielectric surface charges which will show up in the $\mathbf{V}^d$ terms. The dimensions of the vector-matrix quantities appearing in Eqs.(18) and (19) are evident: the vectors $\mathbf{V}^x$ and $\mathbf{q}^x$ are columns of length N_x, and matrices $\mathbf{G}^{xy}$ are N_x by N_y. The partitioned matrix on the LHS of Eq.(19) is thus square, with an equal number of unknowns and equations.

IV. Discrete Approximation of the Green's Functions

In this section the details of the formation of the linear system illustrated in Eq.(19) are given. The first item to be discussed in Section IV.A is typically the most universal of all the coupling terms. One should note that the evaluation of the potential or field at any particular surface element requires summation over all of the known and/or unknown charges in the system. Thus the coupling matrices are typically full, but also well conditioned,[5] due to the nature of the Coulomb interaction.

IV.A. Surface Potential Response to Surface Charge

Consider the potential at a surface element labeled i due to a surface charge distribution. The point in question is a part of the surface itself. Begin with Eq.(11) and write the integral as a sum over surface elements. Within each elemental region of the ds' integral, treat the charge as *constant*. At each point where the potential is to be evaluated, *average* the potential over the linear element. This leaves:

$$V_i \approx -\frac{1}{\varepsilon_o} \sum_j \left[\frac{1}{ds_i} \int_{ds_i} ds \frac{1}{ds_j} \int_{ds_j} ds' \, G(\vec{r},\vec{r}') \right] q_j \,. \tag{20}$$

The total charge on element j, $q_j = 2\pi r_j ds_j \, \sigma(\vec{r}_j)$ has been introduced for each surface element as given in Eq.(16). Write Eq.(20) as

$$V_i^m = \sum_{\substack{j \in s \\ i \in m}} G_{i,j}^{ms} q_j^s \,, \tag{21}$$

to correspond to the vector-matrix notation introduced in Eqs.(15),(17)-(19). Since the potential is only needed at the metal (m) elements, the range of i is restricted to the m partition. For $i \neq j$ the sum-and-average integrals of the Green's function over the finite element can be approximated as

$$G_{i,j}^{ms} \approx -\frac{1}{\varepsilon_o} \, G(r_i,z_i;r_j,z_j) \,, \tag{22}$$

$$i \in m, \, j \in s, \, i \neq j \,.$$

The RHS of Eq.(22) is to be evaluated from the formulae in Eq.(6), making use of the approximate numerical representation of the elliptic integral.[3] This is valid if the surface is smooth, meaning that, approximately, $\left| \vec{r}_i - \vec{r}_j \right| \geq ds_i$ or ds_j. A surface with sharp bends may need refinement of the incrementation. For $i = j$, the diagonal term in Eq.(20) requires a more precise evaluation because of the self-interaction singularity.

The surface element self-interaction term can be approximated as follows. First, since the Green's function is in the near-field limit, the form given in Eq.(8) can be used. Second, the integration and average over the surface element can be done as in the 2D Cartesian case if the dependence on the factor "r" is assumed to be weak compared to the variation of $\vec{r} \approx \vec{r}\,'$ in the argument of the log function. The diagonal coupling term can now be reduced (with some algebra) to

$$G_{i,i}^{ms} = -\frac{1}{4\pi^2 r_i \varepsilon_o} \left(\ln\left(\frac{ds_i}{8r_i}\right) - \frac{3}{2} \right). \tag{23}$$

In the case of a collinear line of equal-length surface elements, the largest relative errors introduced by approximating Eq.(20) by Eq.(22) are 10% for nearest neighbors and 2% for next-nearest neighbors, as derived by analysis of the sum-and-average integrals in Eq.(20). Although it is possible to improve the accuracy by use of coupling terms which depend on the orientation of the individual elements, it does not seem worthwhile, since a systematic reduction in error can be achieved by increasing the number and density of the finite elements.

IV.B. Surface Potential Response to Volume Charge

If there is a space charge in the system, the potential of that charge must be computed from Eq.(9) just as indicated in Eqs.(15) and (17). This involves no self-interaction terms in order to evaluate the potential on the metal surfaces, so the result can be approximated as previously done for the non-diagonal surface-surface terms:

$$V_i^m \approx \sum_{j \in v} G_{i,j}^{mv} \, q_j^v \, ,$$

$$i \in m$$

$$G_{i,j}^{mv} = -\frac{1}{\varepsilon_o} \frac{1}{ds_i} \int_{ds_i} ds \, \frac{1}{2\pi r_j \, dA_j} \int_{dA_j} d^2 r' \, G(\vec{r}, \vec{r}') \, , \qquad (24)$$

$$\approx -\frac{1}{\varepsilon_o} G(r_i, z_i; r_j, z_j) \; .$$

Any improvement in this result would involve incorporating information about the shape of the volume elements next to the surface. As it stands, one might refer to the result in Eq.(24) as a "wire-wire" interaction appropriate for the far-field of the interaction between the finite elements.

IV.C. Imposition of Dielectric Matching Conditions

The match conditions require the evaluation of the normal electric field at the boundaries of dielectrics. For this one must be able to compute the electric field from the surface and volume charges. Consider the field due to all charges in the system, both on surface and in volume, as given by Eq.(12) and its generalization for surface charge similar to Eq.(11):

$$\vec{E}(\vec{r}) = \frac{1}{\varepsilon_o} \int ds' \, \vec{\nabla}_r G(\vec{r}, \vec{r}') \, 2\pi r' \sigma(\vec{r}')$$

$$+ \frac{1}{\varepsilon_o} \int d^2 r' \, \vec{\nabla}_r G(\vec{r}, \vec{r}') \rho(\vec{r}') \, . \qquad (25)$$

The gradient of the Green's function is given in Eq.(13). Choose $\vec{r}$ to be arbitrarily close to the surface of point i, and dot the field with the unit normal of element i to find the component of field normal to that surface element. The result is:

$$\hat{n}_i \cdot \vec{E}(\vec{r}_i) = \frac{1}{\varepsilon_o} \int ds' \, \hat{n}_i \cdot \vec{\nabla}_r G(\vec{r}, \vec{r}') \, 2\pi r' \sigma(\vec{r}')$$

$$+ \frac{1}{\varepsilon_o} \int d^2 r' \, \hat{n}_i \cdot \vec{\nabla}_r G(\vec{r}, \vec{r}') \rho(\vec{r}') \, . \qquad (26)$$

Approximate the integrals in Eq.(26) as sums of terms assuming that the charges are *constant* within each of the surface and volume intervals, as before. This allows the introduction of the elemental charges q_j^s and q_j^v. The result is precisely as symbolized in Eq.(17) with:

$$
\begin{aligned}
{}^nG_{i,j}^{ds} &= \frac{1}{\varepsilon_o} \frac{1}{ds_j} \int_{ds_j} ds'\, \hat{n}_i \cdot \vec{\nabla}_r G(\vec{r}_i, \vec{r}') \\
&\approx \frac{1}{\varepsilon_o} \hat{n}_i \cdot \vec{\nabla}_r G(r_i, z_i; r_j, z_j) \\
i &\neq j, \quad i \in d, \quad j \in s
\end{aligned}
\tag{27}
$$

and

$$
\begin{aligned}
{}^nG_{i,j}^{dv} &= \frac{1}{\varepsilon_o} \frac{1}{2\pi r_j dA_j} \int_{dA_j} d^2 r'\, \hat{n}_i \cdot \vec{\nabla}_r G(\vec{r}_i, \vec{r}') \\
&\approx \frac{1}{\varepsilon_o} \hat{n}_i \cdot \vec{\nabla}_r G(r_i, z_i; r_j, z_j) \\
i &\in d, \quad j \in v
\end{aligned}
\tag{28}
$$

The volume sources are not concerned with self-interaction, but the surface-surface coupling in Eq.(26) must be evaluated for that case. The integral is discontinuous as $\vec{r}$ is carried through the plane of the element. The analytic evaluation of the self-interaction term using the near-field approximation in Eq.(8) gives:

$$
\begin{aligned}
{}^nG_{i,i}^{ss} &= \frac{1}{\varepsilon_o} \frac{1}{ds_i} \int_{ds_i} ds'\, \hat{n}_i \cdot \vec{\nabla} G(\vec{r}_i, \vec{r}'(s')) \\
&\approx \pm \frac{1}{4\pi^2 r_i \varepsilon_o} \frac{\pi}{ds_i}
\end{aligned}
\tag{29}
$$

13

with the positive sign when the unit normal points toward the "computational side" of the element. This is the same as knowing that the electric field about a sheet of positive charge points away from the sheet on both sides and has the magnitude $\sigma / 2\varepsilon_o$ on each side.[1,2] The averaging that was done previously in order to obtain an improved self-interaction term is not necessary here as the limiting values in Eq.(29) are obtained anywhere along the finite surface element. The $\pm$ sign in Eq.(29) will be fixed at $+$ by setting up the unit normal vectors such that they point towards the computational side of the periodic boundary.

Eqs.(27)-(29) fill in the definitions of the $\mathbf{G}^{rx}$ partitions of the matrices as they appear in Eqs.(15) or (17). A detail is the specification and storage of the unit normal vectors. Specifically arrays of the sin and cos of the unit normals are stored at the solution outset and used in the evaluation of the dot products when needed.

The treatment of dielectrics provided here for the purposes of field calculation is that they are replaced with charged boundary layers at their actual surfaces.[1] These charged layers serve to modify the applied fields in order to obtain the correct field strength within the dielectric medium. It is true that there are fundamental reasons why the presence of dielectrics can be analyzed as a vacuum problem with inserted bodies of matter.[1] Since the problems being addressed here are in electrostatics with homogeneous and isotropic media throughout, the formulation is particularly simple. Of course the *whole* problem is not homogeneous and isotropic. All dielectric media will be free of internal charge. The only distributed charge density occurs in the vacuum regions which can contain plasma space charge. The dielectric surfaces, whether between two dielectrics in contact or between a dielectric and the vacuum, will have an unknown amount of surface charge that is sufficient to produce the normal electric field discontinuity required by the macroscopic descriptions. In addition, a prescribed amount of deposited surface charge may be added to represent such charging of dielectric media in contact with a plasma.

Consider, without loss of generality, the following 1D problem in coordinate x. On the right side of the boundary, say for $x > 0$, there is material 1 with permittivity (dielectric constant) ε_1 ; on the left, for $x < 0$ there is material 2 with permittivity ε_2. Let the (x-component) electric field for $x \rightarrow 0^-$ be $E_<$ and the field for $x \rightarrow 0^+$ be $E_>$. The fields are space dependent, so the values near the boundary are to be used. First consider the case with no added surface charge; the dielectric match condition is[1]

$$\varepsilon_2 \, E_< = \varepsilon_1 \, E_> . \tag{30}$$

A "polarization charge" σ^{pol} will be added to the surface to reproduce the jump. Let the field near the boundary be the sum of the fields due to all other sources evaluated at that point, say, E^{other}, and the field due to σ^{pol}. E^{other} must be *continuous* across the boundary. Substituting into Eq.(30) gives:

$$\varepsilon_2 \, E_< = \varepsilon_2 \left(E^{other} - \frac{\sigma^{pol}}{2\varepsilon_o} \right)$$

$$= \varepsilon_1 \, E_> = \varepsilon_1 \left(E^{other} + \frac{\sigma^{pol}}{2\varepsilon_o} \right) \tag{31}$$

from which one solves for σ^{pol}:

$$\sigma^{pol} = \frac{\varepsilon_2 - \varepsilon_1}{\varepsilon_2 + \varepsilon_1} 2\varepsilon_o \, E^{other} . \tag{32}$$

Now write down the expression for the normal component of the electric field at the above boundary, say element i, due to all other charges in the system:

$$E^{other} = \hat{n}_i \cdot \vec{E}(\vec{r}_i) = \sum_{\substack{j \in s \\ j \neq i}} {}^n G_{i,j}^{ds} \, q_j^s + \sum_{j \in v} {}^n G_{i,j}^{dv} \, q_j^v . \tag{33}$$

In order for the sign of Eq.(33) to be correct, the unit normal must point towards positive x, in other words, from medium with ε_2 to medium with ε_1. The ${}^n G_{i,j}^{xy}$ matrices have been defined in Eqs.(27)-(29). Combining Eqs.(32) and (33) and replacing $\sigma^{pol} = q_i^d \, / \, ds_i$ gives

$$0 = \frac{1}{4\pi^2 r_i \varepsilon_o} \frac{\pi}{ds_i} \frac{\varepsilon_1 + \varepsilon_2}{\varepsilon_1 - \varepsilon_2} q_i^d + \sum_{\substack{j \in s \\ j \neq i}} {}^n G_{i,j}^{ds} \, q_j^s + \sum_{j \in v} {}^n G_{i,j}^{dv} \, q_j^v , \tag{34}$$

$$i \in d$$

which is a homogeneous equation in the surface charges similar to the reflective boundary condition partition defined in Section IV.C. A convenient way of expressing Eq.(34) is to define the diagonal of the coupling matrix as:

$$^{n}G_{i,i}^{dd} = \frac{1}{4\pi^2 r_i \varepsilon_o} \frac{\pi}{ds_i} \frac{\varepsilon_1 + \varepsilon_2}{\varepsilon_1 - \varepsilon_2} \quad .$$
$$i \in d$$

$$(35)$$

The limit of $\varepsilon_2 \to \varepsilon_1$ gives a diagonal non-singular system in Eq.(34) and forces all $q_i^d \to 0$, as it should. This completes the dielectric match, except for the inclusion of added surface charge.

Let a deposited surface charge density, $\sigma^{add} = q^{add} / 2\pi r_i ds_i$, be present on the boundary element. This added charge can be displaced away from the boundary surface by a infinitesimal amount and the previous solution for a dielectric match of an uncharged surface can be used again. The displacement must be *towards* the vacuum side of the interface to be consistent with a plasma charge deposition mechanism. In the 1D model above this displacement is characterized by a $\pm$. Thus if the top sign is chosen, dielectric medium 1 is vacuum and $\varepsilon_1 = \varepsilon_o$; if the bottom sign, $\varepsilon_2 = \varepsilon_o$. The field symbolized by E^{other} is now the field due to the charges on all other surface and volume elements, *plus* the field due to the infinitesimally-displaced added charge layer, namely $\mp \sigma^{add} / 2\varepsilon_o$. The charge on the surface element in question is the sum of the polarization and added charges:

$$q^{pol} + q^{add} = q_i^d \quad .$$

$$(36)$$

After eliminating q^{pol} and using the permittivities to remove the $\pm$ sign, one obtains Eq.(34) with an inhomogeneous term:

$$\frac{1}{\varepsilon_1 - \varepsilon_2} \frac{q_i^{add}}{2\pi r_i \, ds_i} = \frac{1}{4\pi^2 r_i \varepsilon_o} \frac{\pi}{ds_i} \frac{\varepsilon_1 + \varepsilon_2}{\varepsilon_1 - \varepsilon_2} q_i^d$$

$$i \in d \qquad\qquad + \sum_{\substack{j \in s \\ j \neq i}} {}^n G_{i,j}^{ds} \, q_j^s + \sum_{j \in v} {}^n G_{i,j}^{dv} \, q_j^v \qquad (37)$$

Of course the diagonal term on the RHS can be defined into the coupling matrices. The LHS of Eq.(37) is the i'th element of the column vector called V^d in Eqs.(17) and (18).

This completes the construction of the linear algebraic equivalent of the integral equation to be solved for the surface charges. Still to do is the case alluded to as the most subtle of the tasks.

IV.D Insulated (Floating) Conducting Bodies

In the study of plasma interaction with surfaces, part of the conducting material in contact with the plasma can be with prescribed voltage and unknown charge, as dealt with earlier in Section IV.A. However a conductor that is electrically insulated will have a known (or determinable) total charge and an unknown voltage and charge distribution on its surface. This would seem to be a formidable problem in potential theory, but the numerical resolution in the context of the surface Green's function methods is quite simple once unveiled.

Rewrite Eq.(19) as

$$\sum_j A_{i,j} x_j = b_i \qquad (38)$$

where $\mathbf{A}$ denotes the square matrix of $\mathbf{G}^{xs}$ coefficients, $\mathbf{x}$ denotes the unknown surface charge vector $\mathbf{q}^s$, and $\mathbf{b}$ the whole RHS vector. Let each insulated conducting body be a subset of the "m" partition in the problem. Give each body a unique label say "k". Let the total charge per length on body k be Q_k. The incorporation of this information into the solution proceeds as follows:

(i) Calculate all of the elements in $\mathbf{A}$ and $\mathbf{b}$ as if the insulated bodies are of specified voltage boundary conditions, as usual in the m partition.

(ii) Search through the rows of $\mathbf{A}$ to find the first member of subpartition k. Say this happens to be row i.

17

(iii) Find the next member of subpartition k. Say that this is row n.

(iv) Replace row i in A and b with

$$A_{i,j} \rightarrow A_{i,j} - A_{n,j} , \quad b_i \rightarrow 0$$
$$\text{for all } j$$

This relation incorporates the condition that the voltage difference between row i and row n (surface elements i and n) is zero, as must be true for a conductor. Remove row i from examination.

(v) Redo the search for members of k, treating row n as the new row i. Repeat (iii) through (v) as long as members of k are found.

(vi) If there is not another member of subpartition k, then replace row i in **A** and **b** with:

$$A_{i,j} = 1, \quad j \in k,$$
$$A_{i,j} = 0, \quad j \notin k,$$
$$b_i = Q_k ,$$

insuring specification of total charge on the subpartition k.

The above must be repeated for all insulated bodies (all distinct k) in the system. One proceeds to solve this transformed **A** and **b** to generate the charges on all the surface elements. Note that no change in dimension or redoing of the interaction matrix element was necessary to carry out the insulated conductor modification.

V. Evaluation of the Fields from the Charges

The solution of the linear system of equations presented by Eq.(19) is done by a full-pivoting Gauss-Jordan elimination code given in "Numerical Recipes"[5]. No problems with the numerical conditioning have been found for any well-formulated problem with up to 700 surface elements using 64-bit arithmetic. The computational time is slower with the larger dimensions, of course.

Finding the potential and electric fields is based on evaluation of the integrals in Eqs.(9), (11), and (25) once the unknown surface charges are found. In the 2D Cartesian procedure[4] the fields were at first approximated by the same methods as presented in Section IV. However, it became obvious in that work that the results were not as smooth as expected near boundary surfaces. One cause of this is that the

evaluation "grid" or sample space is not necessarily related to the finite element setup for the surfaces or the volume charge, if there is one. Thus one can evaluate the fields very close to the surfaces, on the surfaces, or wherever. This difficulty was remedied in the context of the 2D Cartesian work by using the exact analytic field of a 2D finite element with uniform charge as the source term for all the charged surface elements. The more approximate treatment mentioned above is just a modified far-field approximation to this procedure. However in the cylindrically symmetric case being done here, there is no exact analytic solution for the field about a charged finite element that is a figure of rotation about the z axis.

The resolution to this difficulty for the 2D cylindrically symmetric problem was to force a combination of the far-field solution of the cylindrical case with the near-field solution, which is the solution of the uniformly charged Cartesian finite strip. The far-field solution of a circular finite strip element is given precisely by the Green's function in Eq.(6), being the field due to a delta function source (a circular charged wire). The fields about a uniformly charged Cartesian finite strip can be evaluated exactly.[2,4] As mentioned previously though, the volume elements are of unspecified shape and thus not so amenable. The surface treatment for the potential is given now; the electric field is analogous.

Consider a finite surface element strip j which is obtained by rotation about the z axis. This is a conic surface section. The potential due to this strip at the observation point $\bar{r}$ is $V_j(\bar{r})$, the strip element's width is ds_j, its unit normal $\hat{n}_j$, and it is located at $\bar{r}_j$, all specified in cylindrical coordinates. This uniquely specifies the cylindrical charge source element. Denote the functional dependence of the potential on the element parameters by

$$V_j(r,z|r_j,z_j,ds_j,\hat{n}_j) \equiv V^{cs}. \tag{39}$$

where cs denotes "cylindrical strip." Now set up a local 2D Cartesian coordinate system on the element with the positive y axis along $\hat{n}_j$ and the x axis along ds_j, and the origin at $\bar{r}_j$. These (x,y) coordinates are a translation and rotation (by the angle θ of the unit normal) of the cylindrical (r,z) ones. Thus V^{cs} can equally well be written in these coordinates. For convenience, replace the radius of the strip by the curvature, $C_j = 1/r_j$, and denote the dependence of the potential explicitly on C_j and ds_j:

$$V^{cs} \equiv V^{cs}(C_j, ds_j). \tag{40}$$

In terms of these parameters, there are two useful limits. Consider the limit of small surface element width where the finite element reduces to a "circular wire" (cw) of charge:

$$V^{cs}(C_j, ds_j) \xrightarrow[ds_j \to 0]{} V^{cs}(C_j, 0) \equiv V^{cw}. \tag{41}$$

This is the far-field limit of the potential when $|\vec{r} - \vec{r}_j|$ is much greater than ds_j but not necessarily greater than r_j. The other limit is that of an "unrolled" cylindrical strip where the curvature is taken to zero:

$$V^{cs}(C_j, ds_j) \xrightarrow[C_j \to 0]{} V^{cs}(0, ds_j) \equiv V^{ls}. \tag{42}$$

What results here is a "linear strip" (ls) of finite width and infinite depth (in the local z coordinate), for which the exact field solution is known simply in terms of the local (x,y) coordinates. This is a near-field limit which has a constant to be calibrated. The limit of the "linear wire" (lw) must also be used:

$$V^{cs}(C_j, ds_j) \xrightarrow[C_j, ds_j \to 0]{} V^{cs}(0,0) \equiv V^{lw}. \tag{43}$$

The linear wire is the far-field solution to the linear strip when the observation-source separation is much greater than the strip width.

The approximation to be used for the field is to correct the near field of the cw by using the near field of the ls:

$$V^{cs} \approx V^{cw} + V^{ls} - V^{lw} \tag{44}$$

V^{cw} is known exactly as given by the Green's function in Eqs.(6) and (24).

V^{ls} is known[2,4] and the V^{lw} can be obtained from it by taking the limit of zero width. If the (x,y) coordinates are scaled with ds_j, the result is:

$$V^{ls} = -\frac{1}{4\pi^2 r_j \varepsilon_o} q_j^s \left[\ln\left(\frac{ds_j}{R_1}\right) - 1 \right.$$

$$+ y \arctan\left(\frac{1-2x}{2y}\right) + y \arctan\left(\frac{1+2x}{2y}\right)$$

$$+ \frac{1-2x}{4} \ln\left((1/2-x)^2 + y^2\right)$$

$$\left. + \frac{1+2x}{4} \ln\left((1/2+x)^2 + y^2\right) \right]. \tag{45}$$

q_j^s is the total charge on the cylindrical element and R_1 is the constant that sets the zero of the potential field about an infinitely long (in z) x-y strip.[4] The linear wire or far-field limit of Eq.(45) is found to be:

$$V^{lw} = -\frac{1}{4\pi^2 r_j \varepsilon_o} q_j^s \ln\left(\frac{|\vec{r} - \vec{r}_j|}{R_1}\right) \tag{46}$$

The difference of Eqs.(45) and (46) is localized in space to the vicinity of the strip and is the near-field correction. The correction contains quadrupole and higher terms arising from a multipole expansion. Before using this, however, the constant R_1 must be determined as it is no longer valid for the cylindrical geometry. This is done by comparing Eq.(46) with Eq.(8), which is the Green's function giving the field of the circular wire in the limit that the distance from the wire is much less than the radius:

$$V^{cw} \approx -\frac{1}{4\pi^2 r_j \varepsilon_o} q_j^s \ln\left(\frac{|\vec{r} - \vec{r}_j|}{8r_j}\right), \tag{47}$$

$$|\vec{r} - \vec{r}_j| \ll r_j.$$

Thus R_1 is set to $8r_j$ in order that the two limits agree. These formulae are used for the evaluation of the potential due to surface sources.

The potential and field about a space charge element in the volume are difficult to evaluate because of the arbitrary shape. If the volume elements are modeled as being tori of circular cross section, the fields can be approximated using the far-field

limit in which the separation of the evaluation point and the torus is greater than some factor times the effective radius of the elemental cross sectional area dA_j. Define the effective radius r_x as:

$$\pi r_x^2 = dA_j .$$ (48)

For $|\vec{r} - \vec{r}_j| > r_x$, set the potential due to volume element j to

$$V_j(\vec{r}) = \frac{1}{2\pi^2 \varepsilon_o} D_{max}^{-1} K(m) q_j^v ,$$ (49)

based on Eq.(6). For $|\vec{r} - \vec{r}_j| < r_x$, the potential is approximated as a constant:

$$V_j(\vec{r}) \approx -\frac{1}{4\pi^2 r_j \varepsilon_o} \left(\ln\left(\frac{r_x}{8r_j} \right) - \frac{1}{4} \right) q_j^v ,$$ (50)

based on previous analysis, using the near-field limit in Eq.(8).

The electric field is evaluated by much the same analysis as done for the potential. In other words the near-field correction to the "circular wire" is made by using the analytic formulae of the finite strip in (x,y) coordinates.[4] Thus there is a correction of the same form as Eq.(44) made for each component of the electric field. The field about the cw is essentially given by Eq.(13) and the correction is given by the gradients of Eqs.(45) and (46). The electric field due to volume (space) charge is represented by the cw solution when the separation from the volume element exceeds its radius as given in Eq.(48), and by a linearly decreasing function of separation when the separation from the centroid is less than the radius. This is not a perfect solution, but it is found to work well if one is careful about the location of the evaluation grid compared to the grid used to represent the volume charge.

VI. Example Solutions and Discussion

A few examples are given here show the good (and some not-so-good) features of the Green's function method. The prior study of the 2D Cartesian solver[4] contains illustrations that are also representative of the cylindrically symmetric solver.

The first set of computations illustrated in Figs. 1-6 gives the potential and field around a disk capacitor as the number of finite elements is varied on the disks. The disk separation is 1.0m, the disk radii are 1.0m, the plotting field is 2m on a side with 50 points in r and 100 points in z, and the specified voltage is +0.5V on the upper disk and -0.5V on the lower disk. Fig. 1 shows a "wire mesh plot" of the potential for ten finite elements on each disk radius. Note that the total number of unknown finite elements is just twenty, and also that it was not necessary to include any elements on the cylindrical axis since the solution is done in cylindrical symmetry. Some spurious ripples are noted in the potential at the charged elements near the central axis and near the outer edge. A more accurate solution is found by including more elements within each disk radius. In Fig.2 the number of divisions on each disk radius is raised to 25. One notes that the ripples have disappeared. Convergence is confirmed by the results in Fig. 3 where the number of finite elements on each disk is raised to 50.

In Fig. 4 the E_r component of the electric field is shown for the 50-element-per-disk case whose potential is given in Fig. 3. The small "bumps" in the field near the central axis are in fact errors due to the evaluation of the field in a region of both discontinuity in z and near r=0. Fig. 5 shows E_z for this case with 50 elements per disk. In Fig. 6 the magnitude of the field is shown as a contour plot to illustrate how the field is concentrated about the edges of the disks. The absolute value of the field in the central region approaches 1V/m.

The second set of computations is illustrated in Figs. 7-12. A spherically symmetric space charge with a Gaussian distribution in radius is used as the source. The 1/e radius of the charge is 0.25m. The evaluation region is 1m in radius, 2m in height z, and the elements for representation of the volume charge are on a 50 by 100 grid in r and z. Fig. 7 shows the potential over the evaluation volume and Figs. 8 and 9 show the components of the electric field, E_r and E_z. In Fig. 10 the potential is evaluated on a 50 by 100 grid with reduced spacing in the *center* of the full scale region. This is equivalent to a 2X magnification. The same is shown for E_r in Fig. 11 and E_z in Fig. 12. To be noted is that the evaluation grid in the volume is twice as dense as the gird used to represent the space charge. This forces the potential and field evaluation to vary from the center to edge of the incremental volume elements as seen in Eq.(49) and (50) and their generalizations for the electric field components. The oscillation is primarily due to the replacement of the actual square cross section volume elements by the circular approximation as discussed in Section V. The practical rule to avoid the ripple shown in Figs. 11 and 12 is to simply evaluate the potential and/or the electric field on the same grid in the volume as used for the

representation of the charge density, with intermediate values obtained by interpolation. Figs. 7-9 show that this procedure gives smooth and eye-pleasing results.

Any or all of the features of the PE solution discussed in Section IV can be combined in a single problem, including the presence of dielectric media and floating-potential, conducting bodies.

Fortran implementation of this study as well as the prior[4] Cartesian method is available from the author. Contact meriley@sandia.gov by email for information.

Appendix

There is one complication in using any PE solver with a space charge that must be discussed. Consider a parallel plate system with a space charge ρ between the plates, separated by L. This space charge will almost always be the difference between a positive ion density and an electron density -- a plasma in other words. Suppose for the moment that the positive and negative charge densities are equal; thus there is no macroscopic charge and ρ is zero. Now solve the PE with a potential difference ΔV imposed on the plates. The field is just $E = -\Delta V / L$, constant between the plates. Now consider the solution for the response of the particles to this field. The electrons will respond quickly, on a time scale of the electron plasma frequency,[6]

$$\omega_{pe} = \sqrt{n_e e^2 / \varepsilon_o m_e} \tag{A1}$$

which, if the plasma density is high, creates an extremely fast motion which must be resolved with a small time incrementation. Standard notation is used for the symbols in this Appendix. The system will eventually converge to a slowly evolving (quasi-steady-state) solution in which the bulk of the plasma has a very small electric field, with the presence of plasma charge separations near the plates (sheaths) which cancel out the bulk electric field. The thickness of the regions of charge separation is the Debye length,[6]

$$\lambda_D = \sqrt{\varepsilon_o kT_e / e^2 n_e}, \tag{A2}$$

which can be very small compared to the size of the bulk plasma region. In bulk high density plasmas, the electron mobility and diffusion may be shown to drive the electric field to an asymptotic value (ambipolar field),

$$\vec{E} \approx -\frac{kT_e}{e} \frac{\vec{\nabla} n_e}{n_e}. \tag{A3}$$

This is a well known effect and numerical methods exist to help stabilize the solution.[7,8]

Acknowledgments

It should be mentioned that there is a commercial software package available for personal computers and workstations that uses the Green's function method for solving the Poisson equation.[9] Other versions are available for magnetics. Unfortunately the source code was not available so that modifications could be done to incorporate the features required in this study. This code uses refined finite element methods for resolving some of the problems related to the singularities of the Green's functions. That code does not appear to allow for added surface charging of dielectrics, space charge, or insulated conducting elements. However the operation is by "graphical user interface," which greatly facilitates problem definition and solving.

References:

1. Leonard Eyges, "The Classical Electromagnetic Field," Dover Publications, Inc., New York, NY, 1980.

2. P. M.. Morse and H. Feshbach, "Methods of Theoretical Physics," Chs. 7, 10, and 11, McGraw-Hill Book Co., New York, NY, 1953.

3. M. Abramowitz and I. A. Stegun, eds., "Handbook of Mathematical Functions," NBS Appl. Math. Series 55, U.S. Gov. Printing Office, Wash. D.C., June 1964, Ch. 17.

4. M. E. Riley, "Two-Dimensional Green's Function Poisson Solution Appropriate for Feature-Scale Microelectronics Simulations," Sandia National Labs' Technical Report SAND98-0537, March, 1998.

5. W. H. Press, B. P. Flannery, S. A. Teukolsky, and W. T. Vetterling, "Numerical Recipes," Cambridge Univ. Press, New York, NY, 1986.

6. D. C. Montgomery and D. A. Tidman, "Plasma Kinetic Theory," McGraw-Hill Book Co., New York, NY, 1964.

7. P. L. G. Ventzek, R. J. Hoekstra, M. J. Kushner, "2-Dimensional Modeling of High Plasma Density Inductively Coupled Sources for Materials Processing", J. Vac. Sci. Tech. B. 12, 461 (1994).

8. M. J. Kushner, W. Z. Collison, M. J. Grapperhaus, J. P. Holland and M. S. Barnes, "A 3-dimensional Model for Inductively Coupled Plasma Etching Reactors: Azimuthal Symmetry and Coil Properties", J. Appl. Phys. 80, 1337 (1996).

9. "ELECTRO," A two-dimensional Poisson solver sold by Integrated Engineering Software, 46-1313 Border Place, Winnipeg, Manitoba, Canada, R3H 0X4.

Figure 1. This is a "wire mesh plot" of the potential around a disk capacitor whose plates of 1.0m radius are separated by 1.0m.The potential boundary condition is +0.5V on the upper disk and -0.5V on the lower disk The plotting field is 2m on a side with 50 points in r and 100 points in z. Here there are just ten finite elements on each strip. The small ripples in the potential near the center axis on the disks and at the outer edge of the disks is due to the limited resolution of the ten elements. These ripples in the potential cause even more noticeable ripples in the field (not shown).
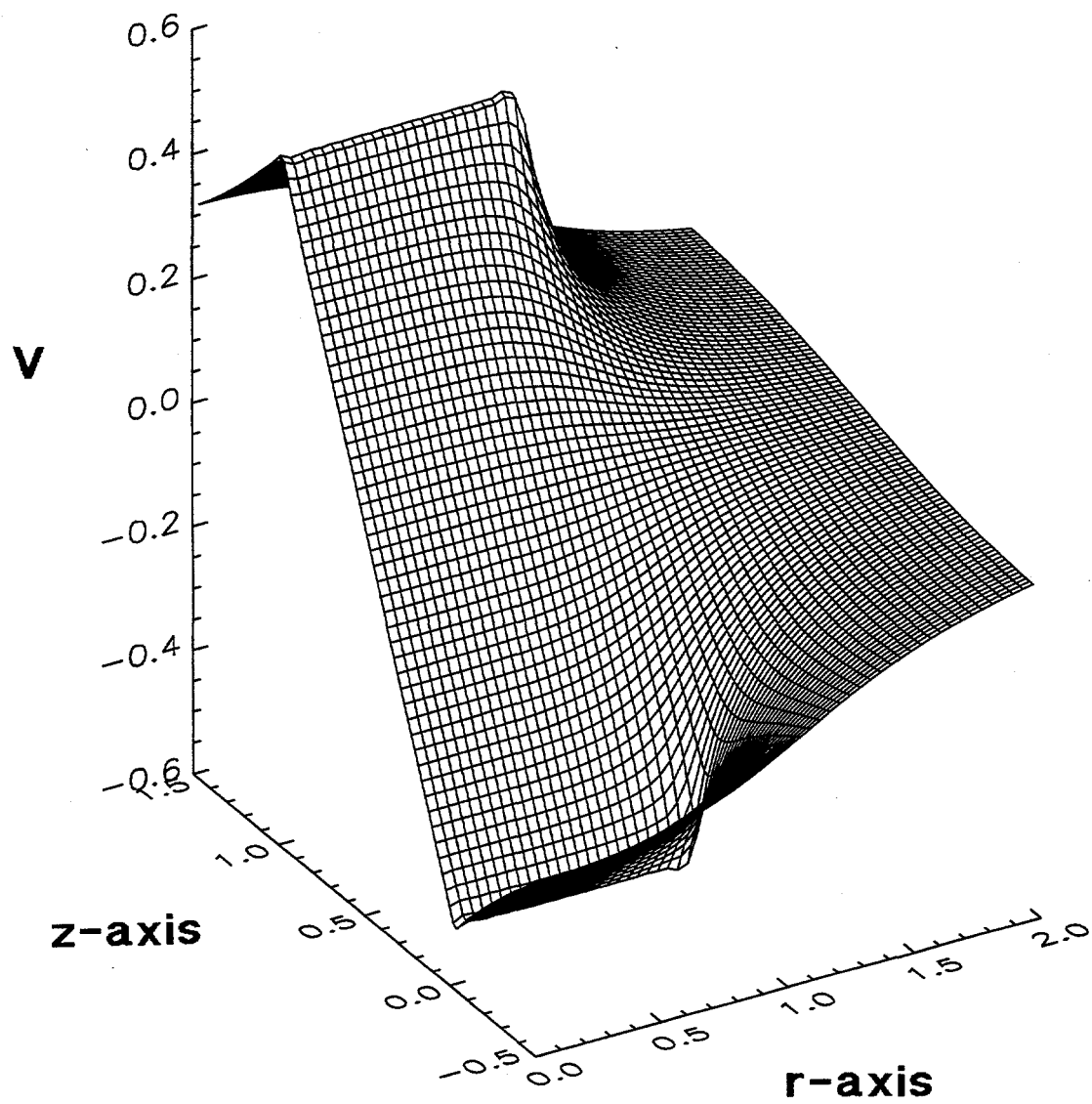
Fig. 1

Figure 2. Same as Fig.1 except in the resolution of the charged disks. Here there are twenty-five finite elements on each disk. The potential at each disk is now more constant in accord with the imposed boundary conditions.
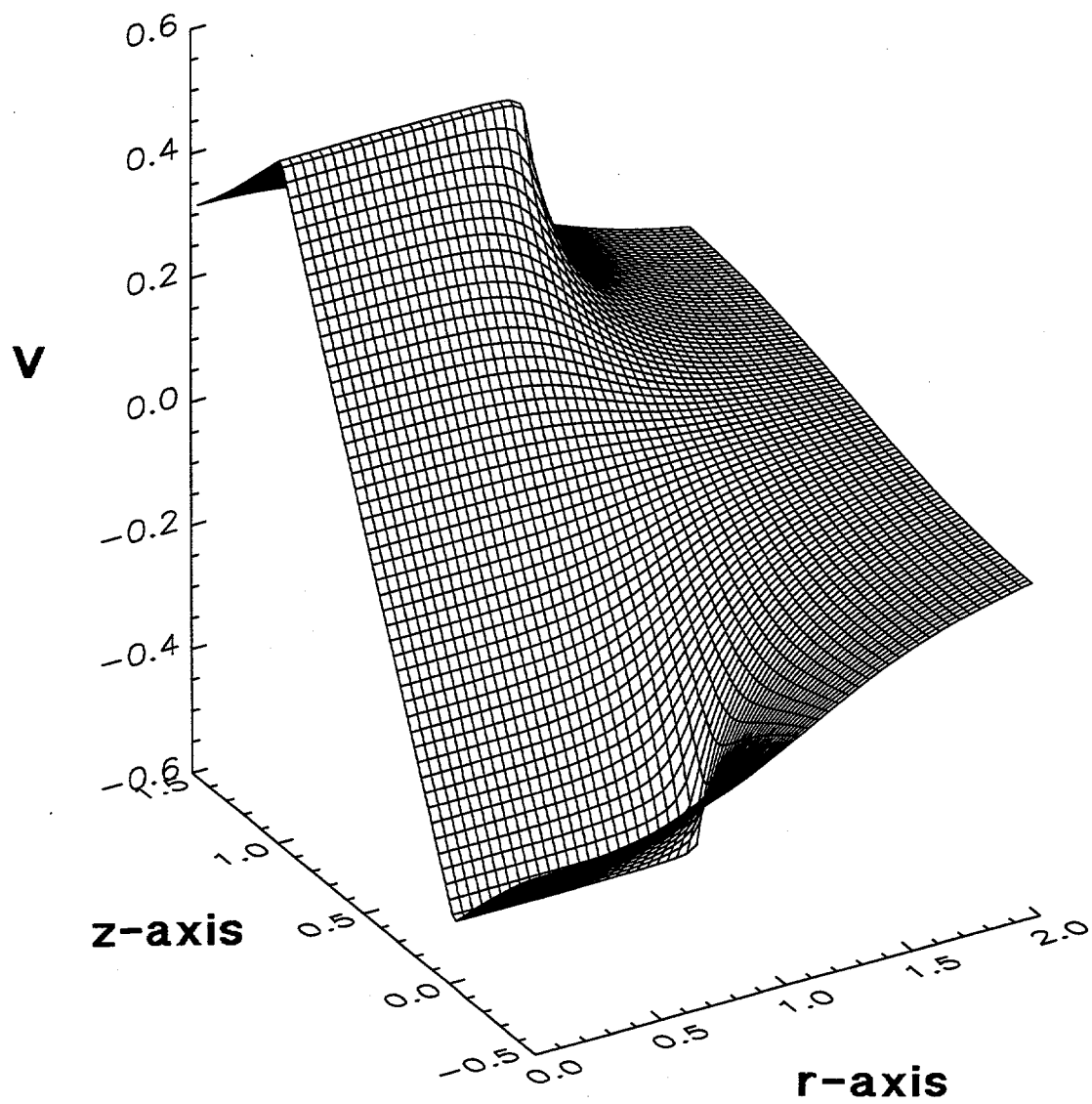
Fig. 2

Figure 3. Same as Figs.1 and 2 except in the resolution of the charged disks. Here there are fifty finite elements on each strip. The potential at each strip is essentially the same as in Fig.2 and demonstrates convergence at eye-resolution level.
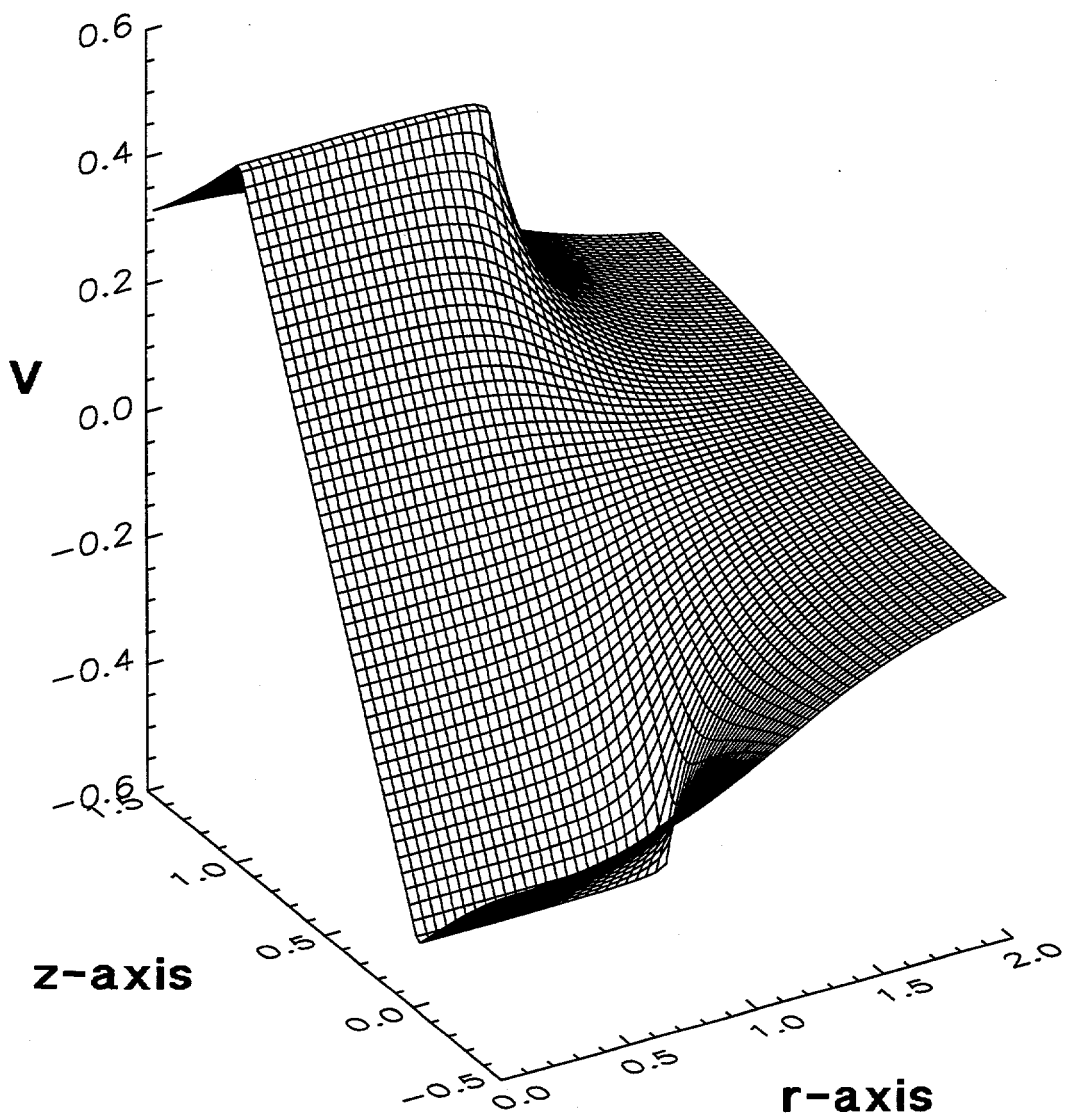
Fig. 3

Figure 4. The radial component of the electric field for the same physical problem as illustrated in Figs.1, 2, and 3. Here there are fifty finite elements on each disk, the same as used for the potential shown in Fig.3. The small ridges that extend outward from the central axis are in fact errors near the axis due to the evaluation of the field in a region of both discontinuity in z and near r=0.
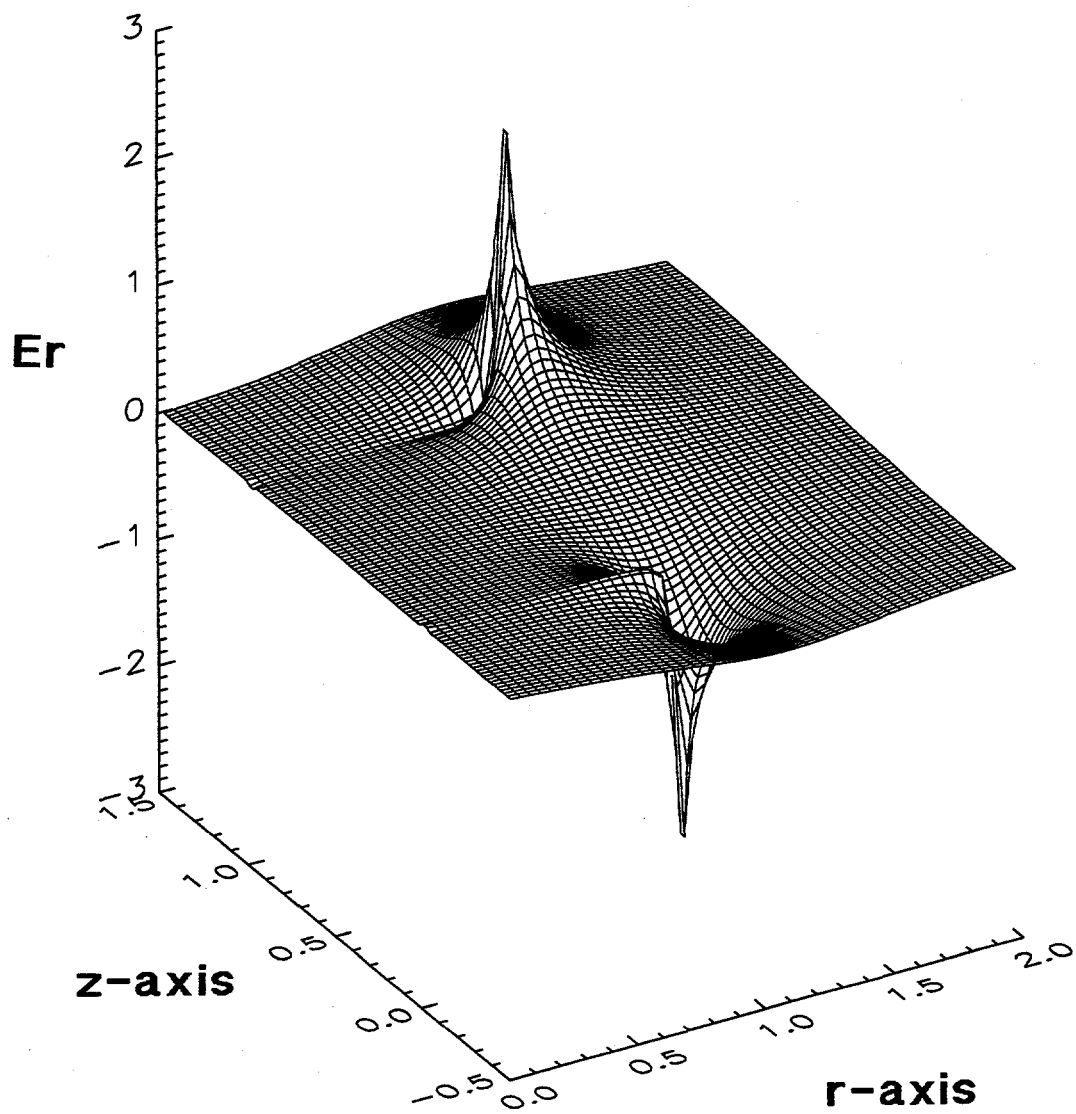
Fig. 4

Figure 5. The z component of the electric field for the same physical problem as illustrated in Figs.1-4.
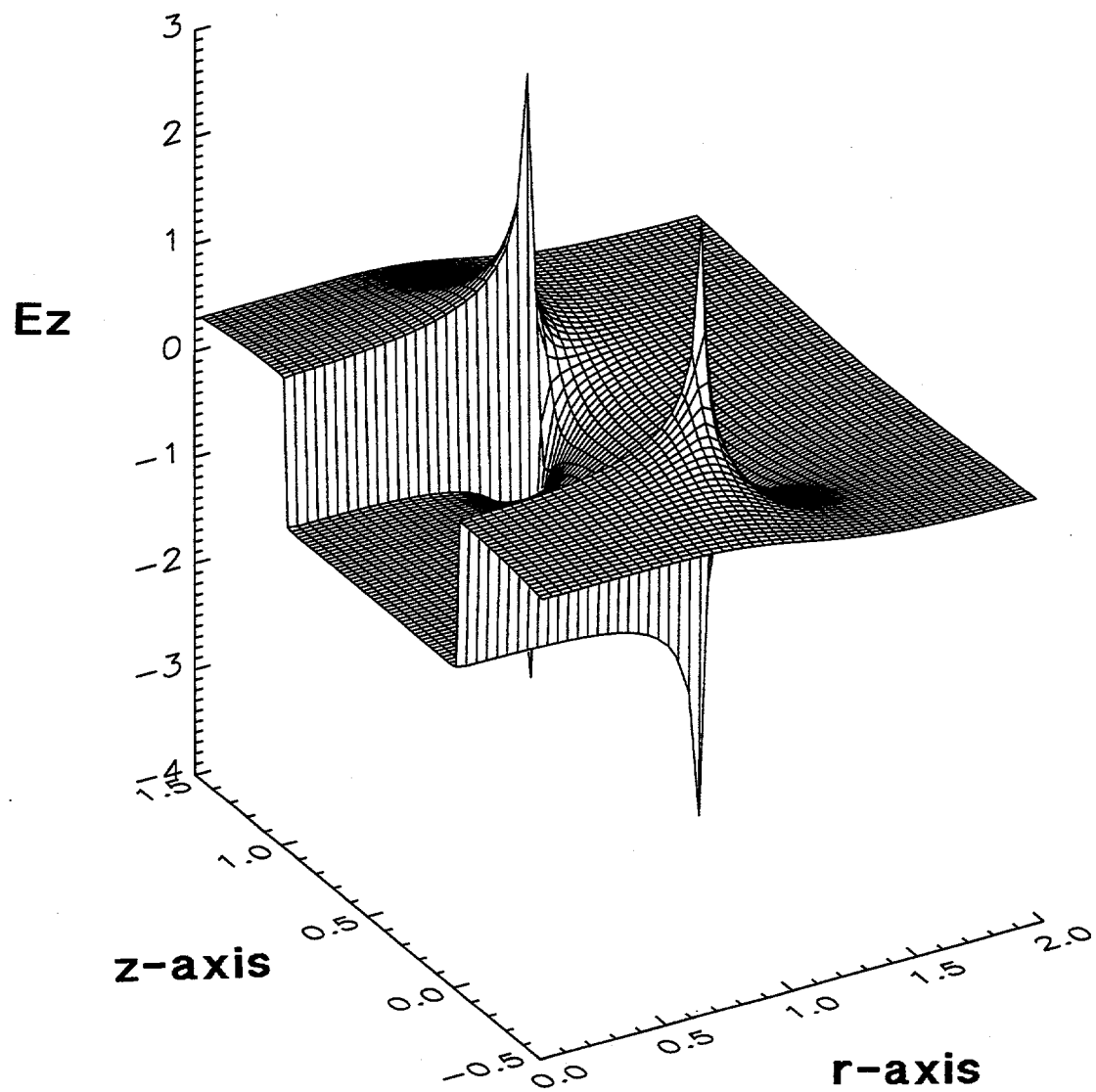
Fig. 5

Figure 6. A contour plot of the magnitude of the electric field given in Figs. 4 and 5. The value in the center of the plates approaches 1V/m.
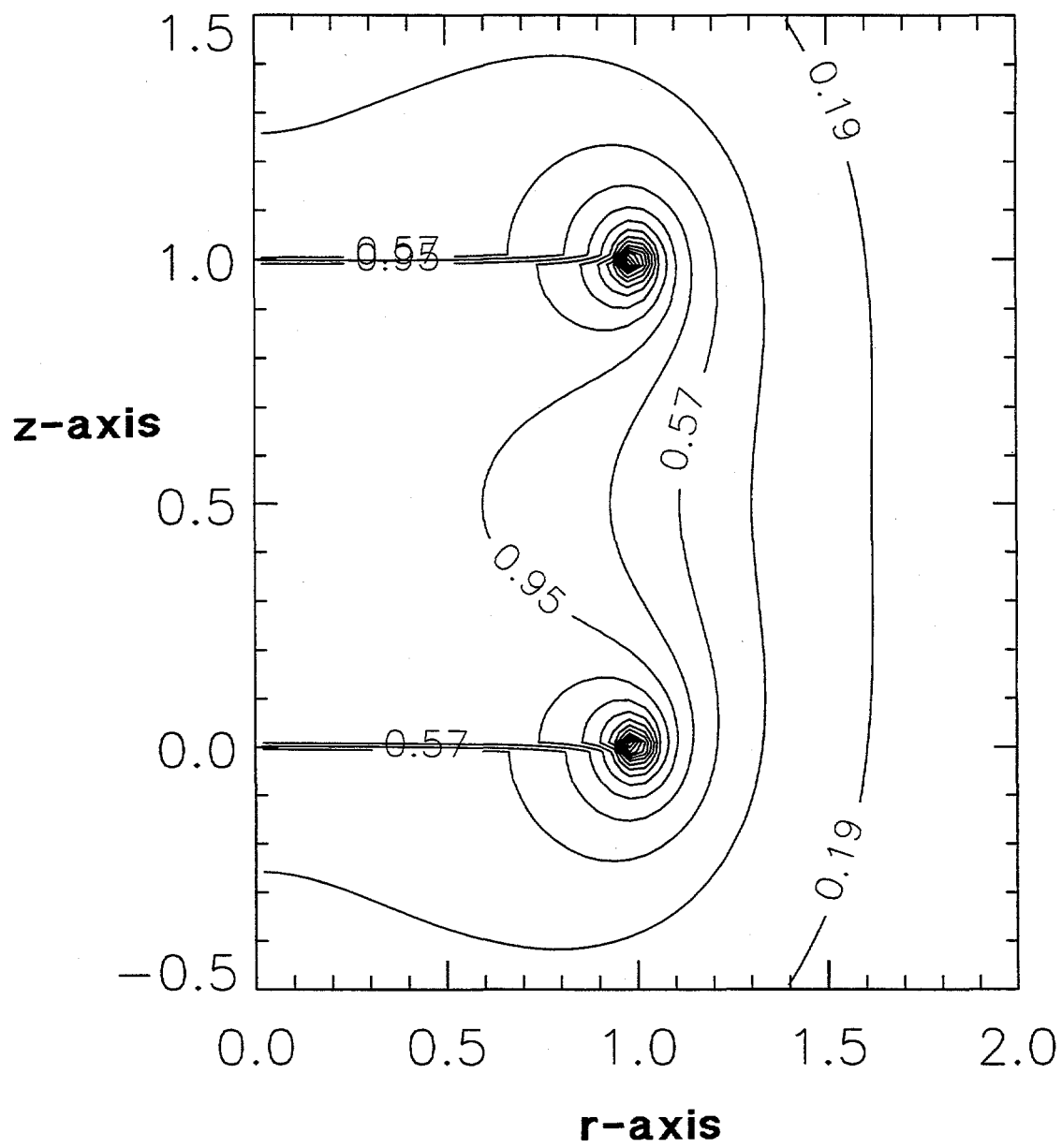
Fig. 6

Figure 7. This is a "wire mesh plot" of the potential due to a *spherically* symmetric space charge distribution whose radial dependence is a Gaussian with 1/e radius of 0.25m. The evaluation region in r and z is a 1m by 2m box. The grid used for the representation of the space charge and for the evaluation of the potential is 50 in r by 100 in z. The important point here is that the potential evaluation and the grid used to compute the space charge in the linear solution are the same.
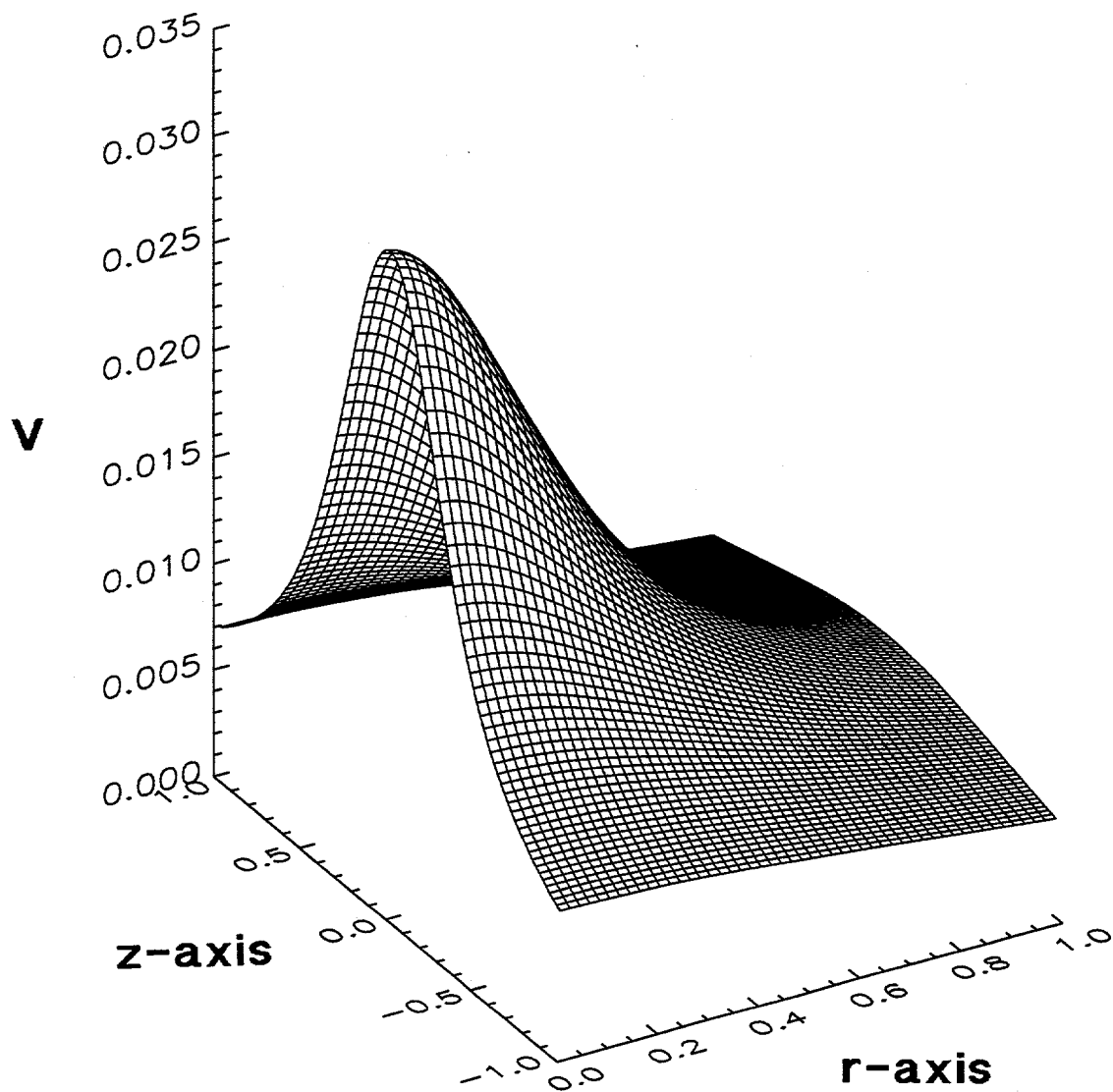
Fig. 7

Figure 8. This is a "wire mesh plot" of the r-component of the electric field corresponding to the potential of Fig. 7. The field is due to a spherical-Gaussian space charge distribution of characteristic radius 0.25m. The evaluation region is a 1m by 2m box. The evaluation grid is 50 by 100, the same as the grid used to represent the volume charge distribution. The important point here is that the grid used to compute the field evaluation and the space charge are the same.
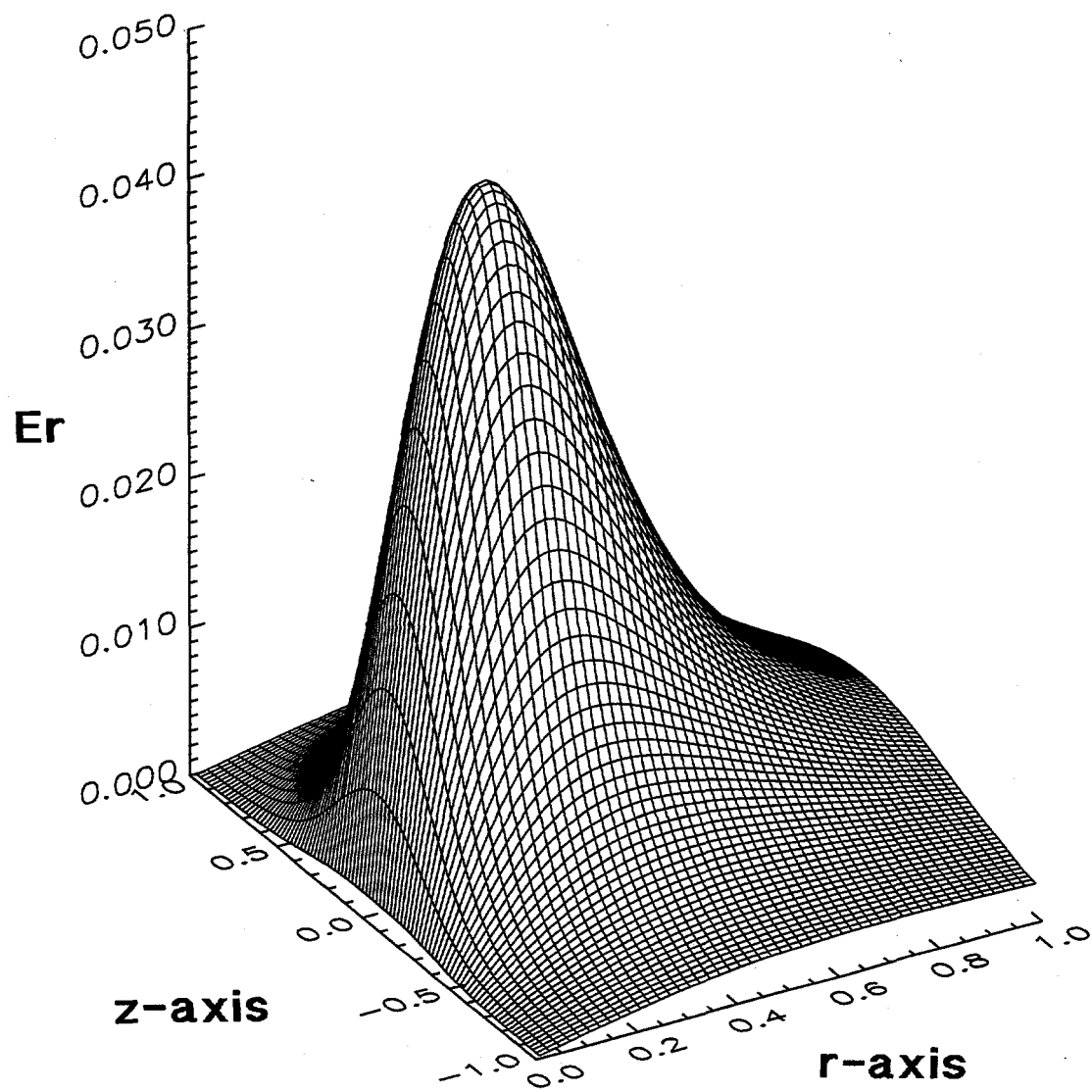
Fig. 8

Figure 9. This is a "wire mesh plot" of the z-component of the electric field corresponding to the potential of Fig. 7. The field is due to a spherical-Gaussian space charge distribution of characteristic radius 0.25m. The evaluation region is a 1m by 2m box. The evaluation grid is 50 by 100, the same as the grid used to represent the volume charge distribution. The important point here is that the grid used to compute the field evaluation and the space charge are the same..
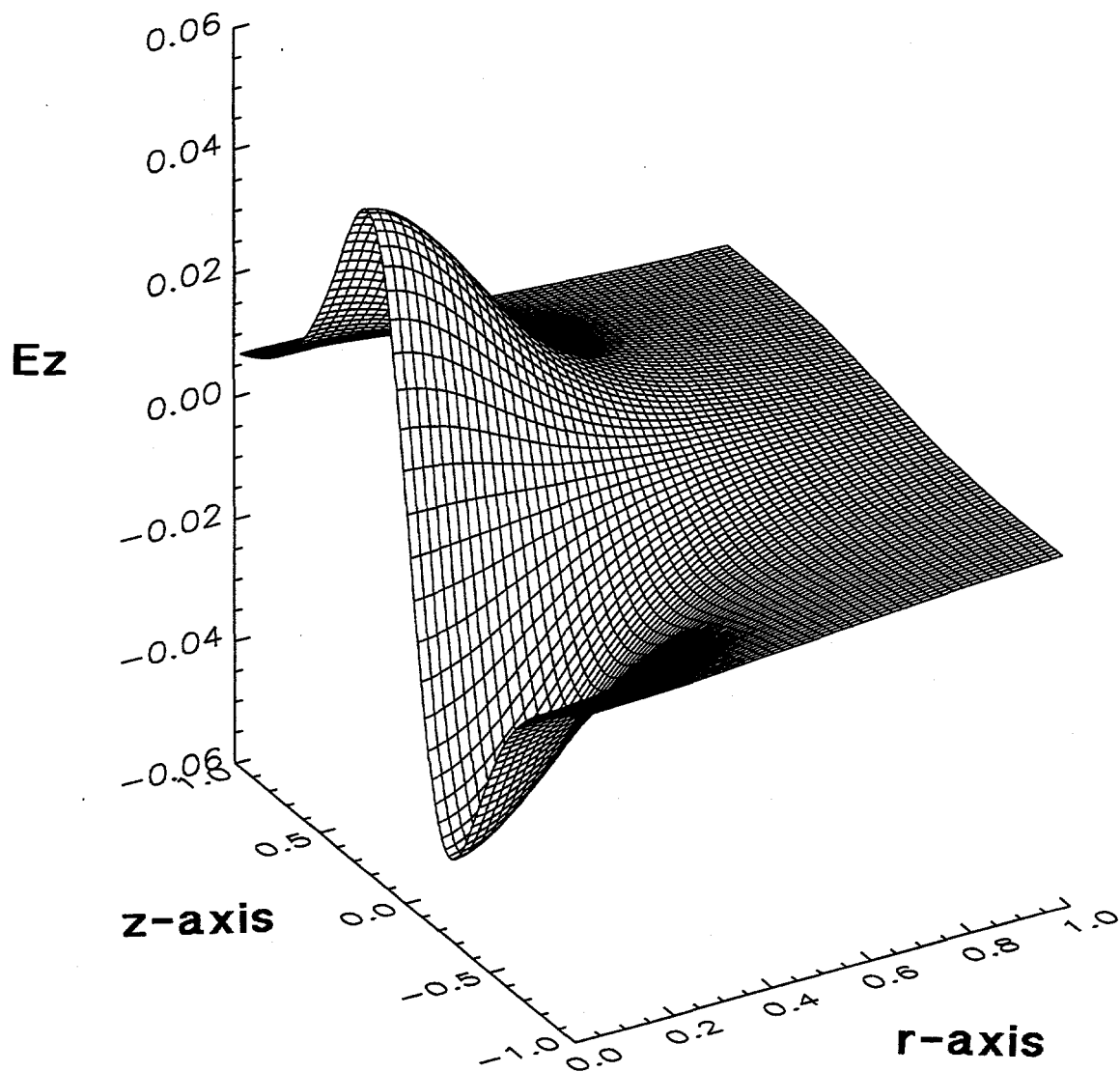
Fig. 9

Figure 10. This is the same potential as shown in Fig.7 evaluated and shown on a 2X magnified scale in the center of the charge distribution. The point here is that the potential evaluation by Eqs.(49) and (50) use a finer grid than used to represent the space charge in the linear solution. This evaluation forces evaluation of the "self-interaction" volume terms to alternate between points near the volume centroid and the edge. This shows most dramatically in the field.
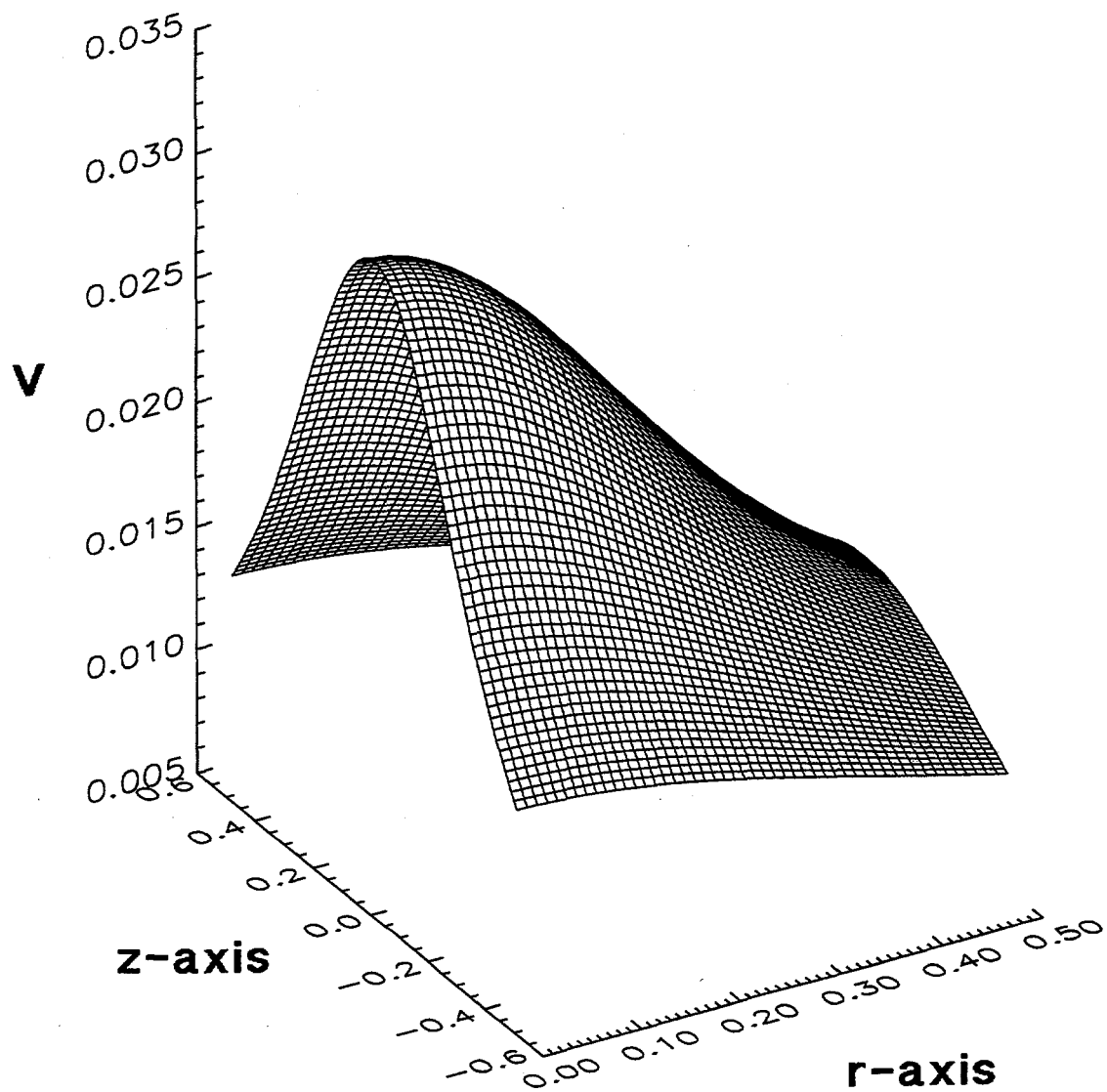
Fig. 10

Figure 11. This is the r-component of the field corresponding to the potential as shown in Fig.10. It is evaluated on a 50 by 100 grid and shown on a 2X magnified scale in the center of the charge distribution. The point here is that the potential evaluation by Eqs.(49) and (50) use a finer grid than used to represent the space charge in the linear solution. The field ripples are due to the alternate evaluation of the field at the center and at the edge of the finite elements, which are assumed to be of circular cross section, but are really squares. In the text it is recommended that field evaluations in the presence of significant amount of space charge be done on the *same* grid as used for the representation of the space charge. This avoids the effect shown here and, at least, gives a more eye-pleasing result.
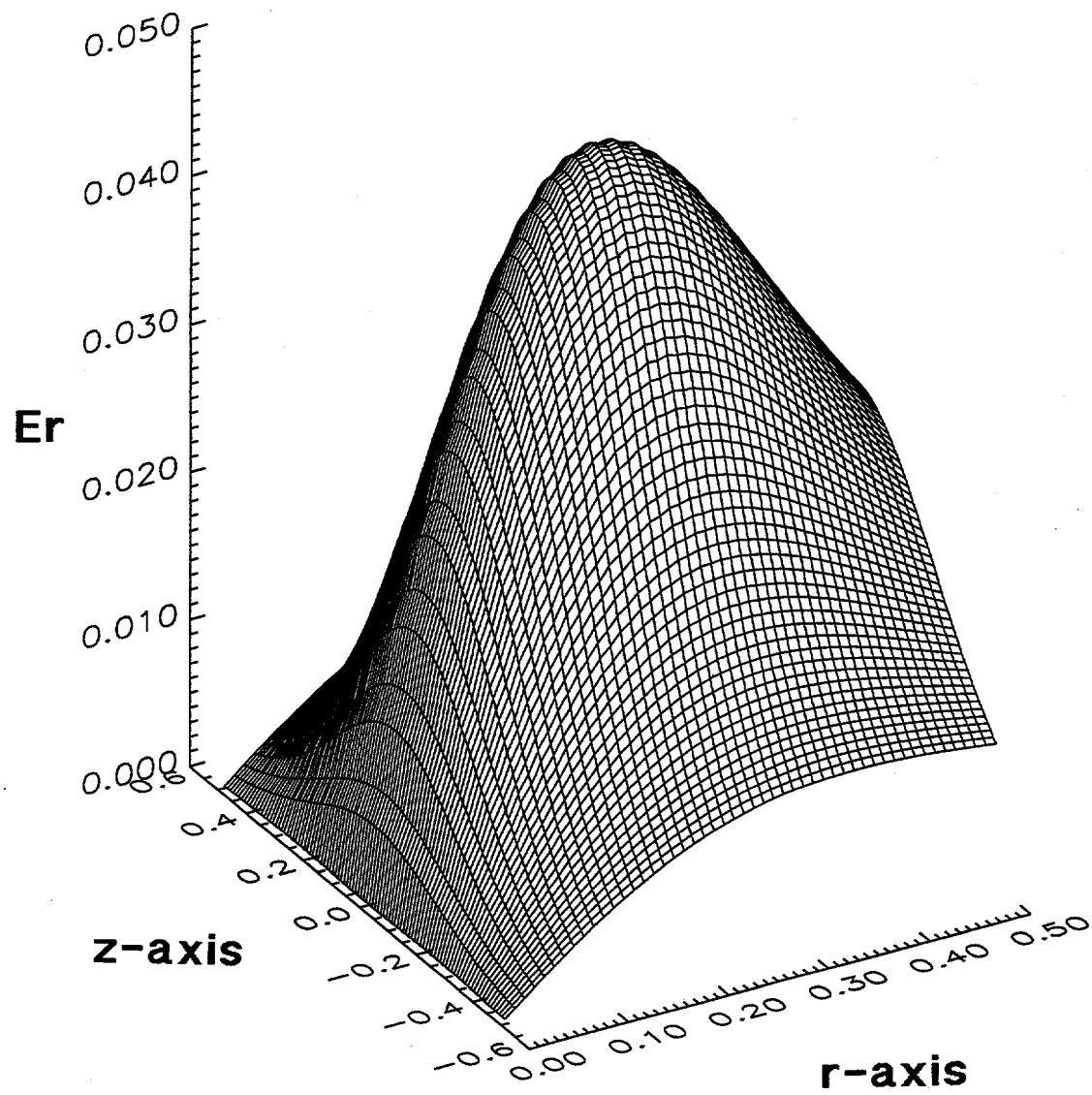
Fig. 11

Figure 12. The z-component of the field corresponding to the potential as shown in Fig.10. It is evaluated on a 50 by 100 grid and shown on a 2X magnified scale in the center of the charge distribution. The point here is that the potential evaluation by Eqs.(49) and (50) use a finer grid than used to represent the space charge in the linear solution. The field ripples are due to the alternate evaluation of the field at the center and at the edge of the finite elements, which are assumed to be of circular cross section, but are really squares. In the text it is recommended that field evaluations in the presence of significant amount of space charge be done on the *same* grid as used for the representation of the space charge. This avoids the effect shown here and, at least, gives a more eye-pleasing result
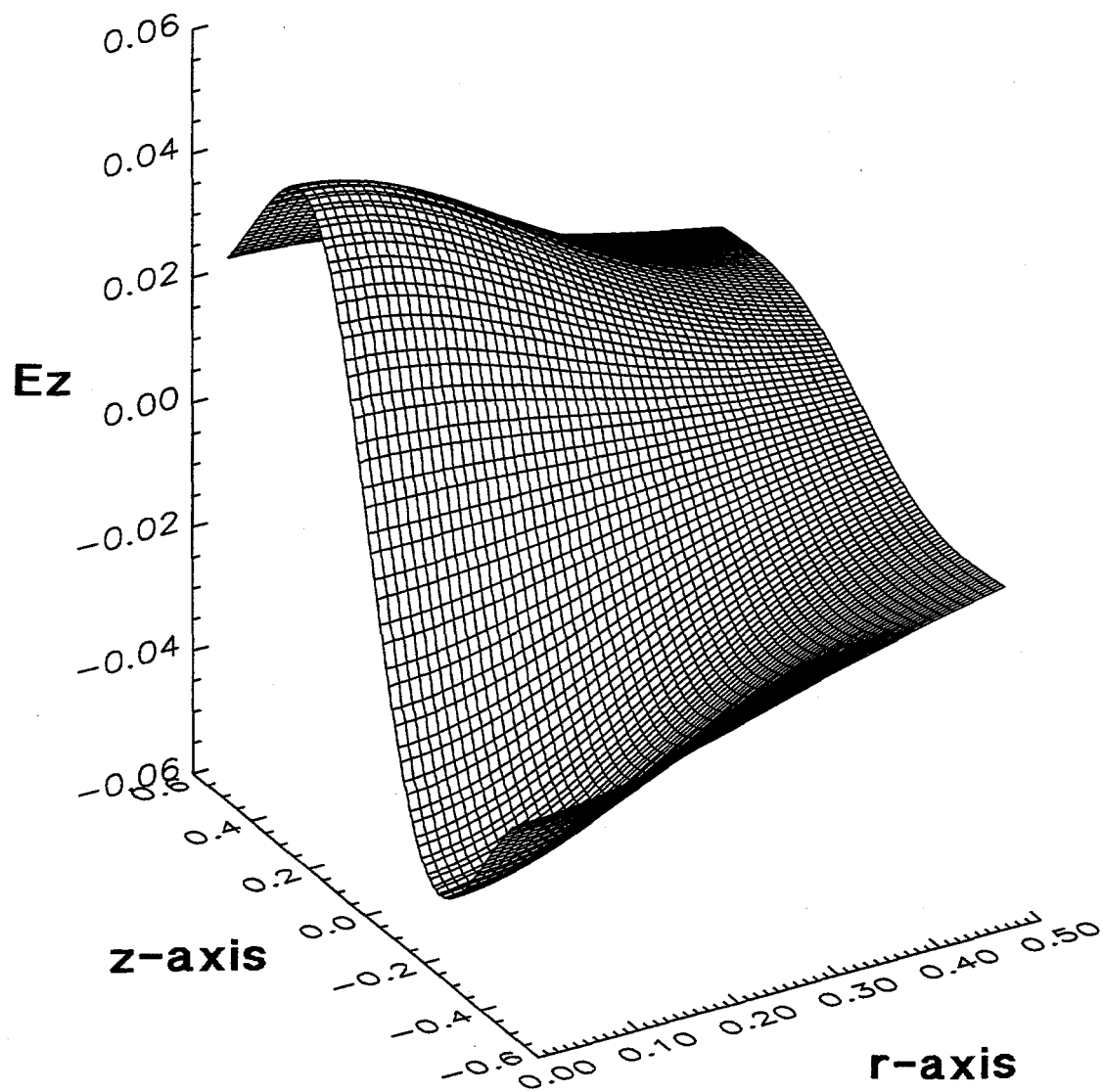
Fig. 12

DISTRIBUTION:

1 Professor Demetre J. Economou
  Department of Chemical Engineering
  University of Houston
  Houston, TX 77204-4792

1 Professor Mark Kushner
  Electrical and Computer Engineering
  University of Illinois
  Urbana, IL 61801

1 Professor Robert T. McGrath
  Engineering Science & Mechanics Department
  227 Hammond Building
  Penn State University
  University Park, PA 16802

1 Dr. Ramana Veerasingam
  MS 0225
  Applied Materials Corporation
  3100 Bowers Ave., Bldg 2
  Santa Clara, CA 95056

1 Robert B. Walker
  MS B268
  Group T-12,
  Los Alamos National Laboratory
  Los Alamos, NM 87545

1 MS 0827 Timothy J. Bartel, 9114

1 MS 0516 John P. Brainard, 1564

1 MS 0827 Robert B. Campbell, 9114

1	MS 0827	Mary L. Hudson, 9114
1	MS 1423	Gregory Hebner, 1128
1	MS 0516	Robert J. Koss, 1564
1	MS 1423	Paul A. Miller, 1128
20	MS 1423	Merle E. Riley, 1128
1	MS 1194	Walter W. Simpson, 9573
1	MS 9018	Central Technical Files, 8940-2
2	MS 0899	Technical Library, 4916
2	MS 0619	Review and Approval Desk, 12690 [For DOE/OSTI]